19th International Conference
ENGINEERING MECHANICS 2013
Svratka, Czech Republic, May 13 – 16, 2013

MODELLING OF THE TURBOCHARGER VIBRATIONS

V. Zeman, Z. Hlaváč *

Abstract: *The paper deals with derivation of the dynamical model of the turbochargers with rotor supported on the two floating ring bearings. The model respects the bearing forces acting upon the journals and floating bearing rings by means of inner and outer oil-films. The gyroscopic effects, external and internal damping of the flexible rotor shaft and the rigid turbine and compressor wheels are respected. The modal analysis and the Campbell diagram is used in the turbocharger linearized model to find the critical speeds.*

Keywords: ***Turbocharger vibrations, eigenvalues, Campbell diagram, critical speeds.***

1. Introduction

The automotive turbochargers work at very high rotor speeds. Therefore the turbocharger vibrations caused by the rotor unbalance is fundamental phenomenon influencing a turbocharger operation. Consider the very high-speed automotive turbocharger (Shäfer (2012)) including the flexible rotor shaft (R), rigid turbine (T) and compressor (C) wheels and two cylindrical floating ring bearings ($\mathrm{B_a}$, $\mathrm{B_b}$) displayed in Fig.1. The lateral-bending behaviour of the isotropic flexible rotor shafts with fixed rigid disks supported on non-isotropic bearings can be modelled by 1-D approach using the finite element method in a fixed coordinate system (Krämer (1993), Genta (2005), Yamamoto & Ishida (2001)). The forces transmitted by oil film bearings can be described for small displacements from static equilibrium position by linearized stiffness and damping matrices depending on the angular rotor velocity ω. Other external and internal damping effects are neglected or are respected approximately. Mostly external vs. internal damping was studied on the fundamental model with rotor mass concentrated in the disk without (Gash & Pfützner (1975), Krämer (1993)) or with gyroscopic effects (Muszińska (2005)). An internal and external damping impact on the stability of the rotors supported on two non-isotropic oil-film bearings was investigated in the paper Zeman & Rendlová (2011). The finite element discretization of the turbocharger rotors has been used for the undamped shaft (Šimek (2013)) or damped rotor (Genta (2005)) using the transfer matrices method. In these works only stiffness and damping effects of one oil-film of bearings was considered. The aim of this article is to present a generally accepted methodology for modelling of the turbocharger rotor supported on two flexible non-isotropic oil-film floating ring bearings respecting two separable oil-films of both bearings and external and internal rotor damping.

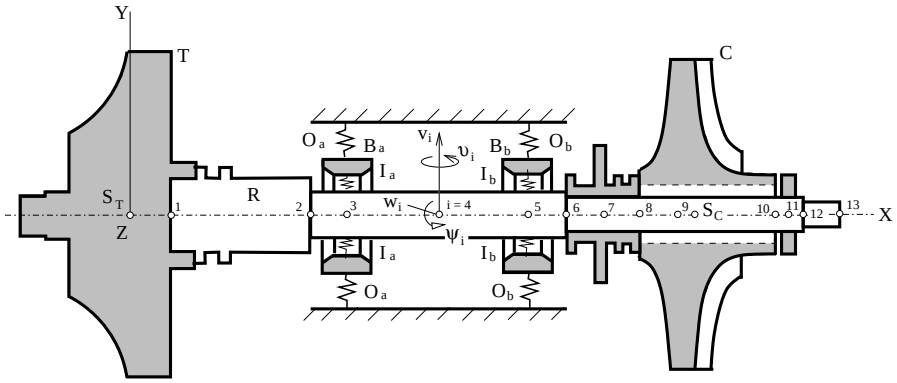

Fig. 1: Computational model of the turbocharger rotor

*Prof. Ing Vladimír Zeman, DrSc., Doc. RNDr. Zdeněk Hlaváč, CSc.: NTIS-New Technologies for Information Society, University of West Bohemia, Univerzitní 22, 306 14 Plzeň, tel. 420 377 63 23 32, e-mail zemanv@kme.zcu.cz

2. Discretization of the rotor shaft

The finite element method (FEM) is applied for a discretization of the flexible rotor shaft with rigid disks. The motion equations can be written in the space of general coordinates

$$\boldsymbol{q}_R = [\ldots, v_i, w_i, \vartheta_i, \psi_i, \ldots]^T , \tag{1}$$

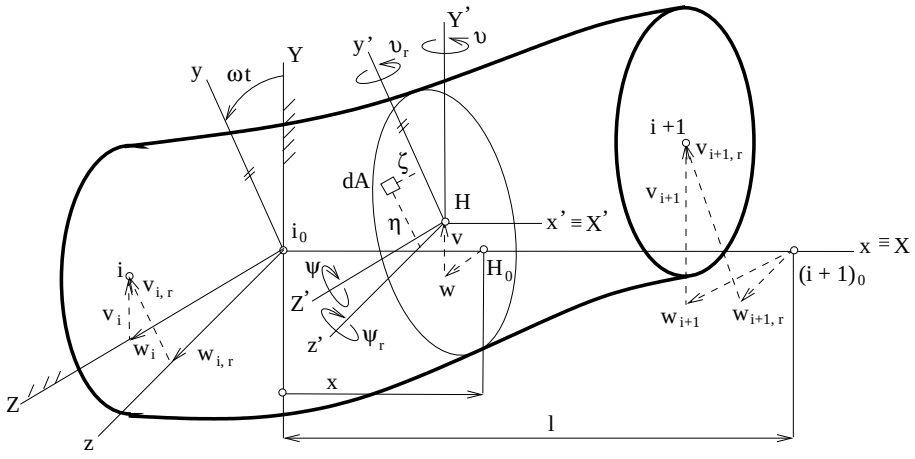

Fig. 2: Prismatic shaft finite element

where v_i, w_i are lateral and ϑ_i, ψ_i angular shaft displacements in the nodal point i in the inertial coordinate system X, Y, Z (Fig.2). The mass $\boldsymbol{M}^{(e)}$, gyroscopic $\omega\boldsymbol{G}^{(e)}$ and stiffness $\boldsymbol{K}^{(e)}$ matrices of the undamped prismatic shaft finite element (FE) between two adjacent nodal points i and $i+1$ can be derived using Lagrange's approach from the identity

$$\frac{\mathrm{d}}{\mathrm{d}t}\left(\frac{\partial E_k^{(e)}}{\partial \dot{\boldsymbol{q}}_{YZ}^{(e)}}\right) - \frac{\partial E_k^{(e)}}{\partial \boldsymbol{q}_{YZ}^{(e)}} + \frac{\partial E_p^{(e)}}{\partial \boldsymbol{q}_{YZ}^{(e)}} = \boldsymbol{M}^{(e)}\ddot{\boldsymbol{q}}_{YZ}^{(e)} + \omega\boldsymbol{G}^{(e)}\dot{\boldsymbol{q}}_{YZ}^{(e)} + \boldsymbol{K}^{(e)}\boldsymbol{q}_{YZ}^{(e)} , \tag{2}$$

where shaft FE displacements are arranged into vector

$$\boldsymbol{q}_{YZ}^{(e)} = [v_i, \psi_i, v_{i+1}, \psi_{i+1}, w_i, \vartheta_i, w_{i+1}, \vartheta_{i+1}]^T . \tag{3}$$

The FE matrices have structure (Byrtus et al. (2010))

$$\boldsymbol{M}^{(e)} = \rho \begin{bmatrix} \boldsymbol{S}_1^{-T}(A\boldsymbol{I}_\Phi + J\boldsymbol{I}_{\Phi'})\boldsymbol{S}_1^{-1} & \boldsymbol{0} \\ \boldsymbol{0} & \boldsymbol{S}_2^{-T}(A\boldsymbol{I}_\Phi + J\boldsymbol{I}_{\Phi'})\boldsymbol{S}_2^{-1} \end{bmatrix} , \tag{4}$$

$$\boldsymbol{G}^{(e)} = 2\rho J \begin{bmatrix} \boldsymbol{0} & \boldsymbol{S}_1^{-T}\boldsymbol{I}_{\Phi'}\boldsymbol{S}_2^{-1} \\ -\boldsymbol{S}_2^{-T}\boldsymbol{I}_{\Phi'}\boldsymbol{S}_1^{-1} & \boldsymbol{0} \end{bmatrix} , \boldsymbol{K}^{(e)} = EJ \begin{bmatrix} \boldsymbol{S}_1^{-T}\boldsymbol{I}_{\Phi''}\boldsymbol{S}_1^{-1} & \boldsymbol{0} \\ \boldsymbol{0} & \boldsymbol{S}_2^{-T}\boldsymbol{I}_{\Phi''}\boldsymbol{S}_2^{-1} \end{bmatrix} , \tag{5}$$

where

$$\boldsymbol{I}_\Phi = \int_0^l \boldsymbol{\Phi}^T(x)\boldsymbol{\Phi}(x)\mathrm{d}x,\ \boldsymbol{I}_{\Phi'} = \int_0^l \boldsymbol{\Phi'}^T(x)\boldsymbol{\Phi'}(x)\mathrm{d}x,\ \boldsymbol{I}_{\Phi''} = \int_0^l \boldsymbol{\Phi''}^T(x)\boldsymbol{\Phi''}(x)\mathrm{d}x,$$

$$\boldsymbol{\Phi}(x) = [1, x, x^2, x^3],\ \boldsymbol{S}_{1,2} = \begin{bmatrix} 1 & 0 & 0 & 0 \\ 0 & \pm 1 & 0 & 0 \\ 1 & l & l^2 & l^3 \\ 0 & \pm 1 & \pm 2l & \pm 3l^2 \end{bmatrix} , \text{ sign } + \text{ for } \boldsymbol{S}_1, \text{ sign } - \text{ for } \boldsymbol{S}_2 .$$

Every shaft element of length l is determined by mass density ρ, cross-section area A, second moment of cross-section area J and Young's modulus E.

External damping forces, acting on the shaft FE, depend on the lateral absolute velocity. The Rayleigh dissipation function in the inertial coordinate system X, Y, Z is expressed as

$$R_E^{(e)} = \frac{1}{2}\int_0^l [b_{EY}\dot{v}^2(x,t) + b_{EZ}\dot{w}^2(x,t)]\mathrm{d}x , \tag{6}$$

where b_{EY} and b_{EZ} [kgm^{-1}s^{-1}] are coefficients of viscous damping per unit length of the shaft FE. Its lateral deformations along the shaft FE are approximated polynomial in the form

$$v(x,t) = \boldsymbol{\Phi}(x)\boldsymbol{S}_1^{-1}[v_i, \psi_i, v_{i+1}, \psi_{i+1}]^T, w(x,t) = \boldsymbol{\Phi}(x)\boldsymbol{S}_2^{-1}[w_i, \vartheta_i, w_{i+1}, \vartheta_{i+1}]^T. \tag{7}$$

The *external damping matrix* $\boldsymbol{B}_E^{(e)}$ results from identity

$$\frac{\partial R_E^{(e)}}{\partial \dot{\boldsymbol{q}}_{YZ}^{(e)}} = \boldsymbol{B}_E^{(e)}\dot{\boldsymbol{q}}_{YZ}^{(e)}, \ \boldsymbol{B}_E^{(e)} = \begin{bmatrix} b_{EY}\boldsymbol{S}_1^{-T}\boldsymbol{I}_\Phi\boldsymbol{S}_1^{-1} & \boldsymbol{0} \\ \boldsymbol{0} & b_{EZ}\boldsymbol{S}_2^{-T}\boldsymbol{I}_\Phi\boldsymbol{S}_2^{-1} \end{bmatrix}. \tag{8}$$

The normal stress σ_I generated by internal damping forces in axial direction can by expressed as proportional to longitudinal strain velocity (Gash & Pfützner (1975)) in the form $\sigma_I = b_I E\dot{\varepsilon}_x$, where b_I is coefficient of viscous internal (material) damping and ε_x is longitudinal unit deformation. The power of the elementary damping force transmitted by surface element $\mathrm{d}A$ of cross-section is $\sigma_I \mathrm{d}A\dot{\varepsilon}_x\mathrm{d}x$, where $\dot{\varepsilon}_x\mathrm{d}x$ is strain rate. The corresponding Rayleigh dissipation function in rotating coordinate system x, y, z ($x \equiv X$) is expressed as

$$R_I^{(e)} = \frac{1}{2}\int_0^l \int_A b_I E\dot{\varepsilon}\mathrm{d}A\mathrm{d}x. \tag{9}$$

Providing small angular flexural cross-section displacements longitudinal unit deformation in arbitrary point (η, ζ) of shaft cross-section is

$$\varepsilon_x = -\eta\frac{\partial^2 v_r}{\partial x^2} - \zeta\frac{\partial^2 w_r}{\partial x^2}. \tag{10}$$

The lateral shaft FE deformations v_r, w_r in the rotating coordinate frame x, y, z can be approximated polynomial in the similar form to (7)

$$v_r(x,t) = \boldsymbol{\Phi}(x)\boldsymbol{S}_1^{-1}[v_{i,r}, \psi_{i,r}, v_{i+1,r}, \psi_{i+1,r}]^T, \ w_r(x,t) = \boldsymbol{\Phi}(x)\boldsymbol{S}_2^{-1}[w_{i,r}, \vartheta_{i,r}, w_{i+1,r}, \vartheta_{i+1,r}]^T, \tag{11}$$

where lateral displacements marked with subscript i, r, $i+1, r$ correspond to nodal point i, $i+1$. The angular flexural cross-section displacements around rotating axes $y' \parallel y$, $z' \parallel z$ are marked ϑ_r and ψ_r (Fig.2). The *internal damping matrix* $\boldsymbol{B}_I^{(e)}$ results from identity

$$\frac{\partial R_I^{(e)}}{\partial \dot{\boldsymbol{q}}_{yz}} = \boldsymbol{B}_I^{(e)}\dot{\boldsymbol{q}}_{yz}^{(e)}, \tag{12}$$

where shaft FE displacements in rotating coordinate system are arranged into vector

$$\boldsymbol{q}_{yz}^{(e)} = [v_{i,r}, \psi_{i,r}, v_{i+1,r}, \psi_{i+1,r}, w_{i,r}, \vartheta_{i,r}, w_{i+1,r}, \vartheta_{i+1,r}]^T. \tag{13}$$

According to (9) up to (13) we get internal damping matrix in the rotating coordinate system

$$\boldsymbol{B}_I^{(e)} = b_I E J \begin{bmatrix} \boldsymbol{S}_1^{-T}\boldsymbol{I}_{\Phi''}\boldsymbol{S}_1^{-1} & \boldsymbol{0} \\ \boldsymbol{0} & \boldsymbol{S}_2^{-T}\boldsymbol{I}_{\Phi''}\boldsymbol{S}_2^{-1} \end{bmatrix}. \tag{14}$$

We use the relations

$$\boldsymbol{q}_{yz}^{(e)} = \boldsymbol{T}(t)\boldsymbol{q}_{YZ}^{(e)}, \ \dot{\boldsymbol{q}}_{yz}^{(e)} = \dot{\boldsymbol{T}}(t)\boldsymbol{q}_{YZ}^{(e)} + \boldsymbol{T}(t)\dot{\boldsymbol{q}}_{YZ}^{(e)} \tag{15}$$

between displacement and velocity vectors of shaft FE nodal points in the rotating x, y, z and the inertial X, Y, Z coordinate systems. The internal damping force vector $(\boldsymbol{f}_I^{(e)})_{yz} = -\boldsymbol{B}_I^{(e)}\dot{\boldsymbol{q}}_{yz}^{(e)}$ on the right side of the shaft FE motion equations is transformed to the inertial coordinate system

$$(\boldsymbol{f}_I^{(e)})_{YZ} = -\boldsymbol{T}^T(t)\boldsymbol{B}_I^{(e)}\dot{\boldsymbol{q}}_{yz}^{(e)}. \tag{16}$$

According to (3) and (13) the transformation matrix is

$$\boldsymbol{T}(t) = \begin{bmatrix} \boldsymbol{E}\cos\omega t & \boldsymbol{D}\sin\omega t \\ -\boldsymbol{D}\sin\omega t & \boldsymbol{E}\cos\omega t \end{bmatrix}, \ \boldsymbol{D} = \mathrm{diag}[1, -1, 1, -1] \tag{17}$$

and $\boldsymbol{E}$ is unit matrix of order four. Using relations (15) and (16) we get

$$(\boldsymbol{f}_I^{(e)})_{YZ} = -\boldsymbol{T}^T(t)\boldsymbol{B}_I^{(e)}\boldsymbol{T}^T\dot{\boldsymbol{q}}_{YZ}^{(e)} - \boldsymbol{T}^T(t)\boldsymbol{B}_I^{(e)}\dot{\boldsymbol{T}}(t)\boldsymbol{q}_{YZ}^{(e)}\,. \tag{18}$$

It is possible to achieve relations

$$\boldsymbol{T}^T(t)\boldsymbol{B}_I^{(e)}\boldsymbol{T}(t) = \boldsymbol{B}_I^{(e)}\,,\ \boldsymbol{T}^T(t)\boldsymbol{B}_I^{(e)}\dot{\boldsymbol{T}}(t) = \omega\boldsymbol{C}^{(e)} \tag{19}$$

whereas matrix

$$\omega\boldsymbol{C}^{(e)} = \omega b_I E J \begin{bmatrix} \boldsymbol{0} & \boldsymbol{S}_1^{-T}\boldsymbol{I}_{\Phi''}\boldsymbol{S}_1^{-1}\boldsymbol{D} \\ -\boldsymbol{D}\boldsymbol{S}_1^{-T}\boldsymbol{I}_{\Phi''}\boldsymbol{S}_1^{-1} & \boldsymbol{0} \end{bmatrix}, \tag{20}$$

for constant angular rotor velocity ω is in time the constant antisymmetrical matrix. This so-called circulatory matrix is linearly dependent on shaft angular velocity. Mathematical model of the shaft FE bending vibration in inertial coordinate system according to (2), (8) and after translation of the vector $(\boldsymbol{f}_I^{(e)})_{YZ}$ expressed in (18) on the left side of the shaft FE motion equations has the form

$$\boldsymbol{M}^{(e)}\ddot{\boldsymbol{q}}_{YZ}^{(e)} + (\boldsymbol{B}_E^{(e)} + \boldsymbol{B}_I^{(e)} + \omega\boldsymbol{G}^{(e)})\dot{\boldsymbol{q}}_{YZ}^{(e)} + (\boldsymbol{K}^{(e)} + \omega\boldsymbol{C}^{(e)})\boldsymbol{q}_{YZ}^{(e)} = \boldsymbol{0}\,. \tag{21}$$

It's evident that external damping generates dissipative symmetrical damping matrix $\boldsymbol{B}_E^{(e)}$ and internal damping generates dissipative symmetrical damping matrix $\boldsymbol{B}_I^{(e)}$ and antisymmetrical circulatory matrix $\omega\boldsymbol{C}^{(e)}$.

3. Equations of rotor motion

The motion equations of the automotive turbocharger including the rotor shaft, turbine wheel, compressor wheel, seal and thrust rings and two rotating floating ring bearings (Fig.1) will be derived in the configuration space defined in the form

$$\boldsymbol{q} = [\boldsymbol{q}_R^T, \boldsymbol{q}_B^T]^T = [\ldots, v_i, w_i, \vartheta_i, \psi_i, \ldots, v_a, w_a, v_b, w_b]^T\,, \tag{22}$$

where vector $\boldsymbol{q}_R$ of dimension $4N$ ($N =$ number of rotor shaft nodal points) was defined in (1) and the subvector

$$\boldsymbol{q}_B = [v_a, w_a, v_b, w_b]^T \tag{23}$$

expresses lateral displacements of the rigid bearing rings R_a (left) and R_b (right) with respect to frame. The matrices of the shaft element defined in equation (21) must be transformed in the form

$$\boldsymbol{X}_e = \boldsymbol{P}^T\boldsymbol{X}^{(e)}\boldsymbol{P}\,,\ \boldsymbol{X}^{(e)} = \boldsymbol{M}^{(e)}, \boldsymbol{B}_E^{(e)}, \boldsymbol{B}_I^{(e)}, \boldsymbol{G}^{(e)}, \boldsymbol{K}^{(e)}, \boldsymbol{C}^{(e)}\,, \tag{24}$$

where permutation matrix $\boldsymbol{P}$ corresponds to relation

$$\boldsymbol{q}_{YZ}^{(e)} = \boldsymbol{P}\boldsymbol{q}_e\,,\ \boldsymbol{q}_e = [v_i, w_i, \vartheta_i, \psi_i, v_{i+1}, w_{i+1}, \vartheta_{i+1}, \psi_{i+1}]^T\,.$$

The structure of the all global rotor shaft matrices without disks and bearings is given by following scheme

$$\boldsymbol{X}_R = \sum_e \mathrm{diag}[\boldsymbol{0}, \boldsymbol{X}_e, \boldsymbol{0}]\,,\ \boldsymbol{X}_R = \boldsymbol{M}_R, \boldsymbol{B}_R^{(E)}, \boldsymbol{B}_R^{(I)}, \boldsymbol{G}_R, \boldsymbol{K}_R, \boldsymbol{C}_R \in R^{4N,4N} \tag{25}$$

with block matrices $\boldsymbol{X}_e$ determined in (24).

The mass, gyroscopic and external damping matrices of the axisymmetric rigid disk fast linked with the rotor shaft in nodal point i can be derived using Lagrange's approach based on the kinetic energy and dissipation function. The kinetic energy of the disk includes of the lateral and rotational parts

$$E_k^{(D)} = \frac{1}{2}m[(\dot{v}_i - a\dot{\psi}_i)^2 + (\dot{w} + a\dot{\vartheta}_i)^2] + \frac{1}{2}I_0(\omega + \dot{\vartheta}_i\psi_i)^2 + \frac{1}{2}I(\dot{\vartheta}_i^2 + \dot{\psi}_i^2)\,, \tag{26}$$

where m is the mass, a is the distance of the disk mass center from nodal point i (see Fig.1) and I, I_0 are the transverse and polar mass inertia moments. The disk dissipation function is

$$R^{(D)} = \frac{1}{2} b_l (\dot{v}_i^2 + \dot{w}_i^2) + \frac{1}{2} b_c (\dot{\vartheta}_i^2 + \dot{\psi}_i^2) \,, \tag{27}$$

where b_l, b_c are lateral and circulant damping coefficients, respectively. The mass $\boldsymbol{M}_D$, external damping $\boldsymbol{B}_D$ and gyroscopic $\omega \boldsymbol{G}_D$ matrices of the balanced disk follow from identity

$$\frac{\mathrm{d}}{\mathrm{d}t} \left(\frac{\partial E_k^{(D)}}{\partial \dot{\boldsymbol{q}}_i} \right) - \frac{\partial E_k^{(D)}}{\partial \boldsymbol{q}_i} + \frac{\partial R^{(D)}}{\partial \dot{\boldsymbol{q}}_i} = \boldsymbol{M}_D \ddot{\boldsymbol{q}}_i + (\boldsymbol{B}_D + \omega \boldsymbol{G}_D) \dot{\boldsymbol{q}}_i \,, \tag{28}$$

where $\boldsymbol{q}_i = [v_i, w_i, \vartheta_i, \psi_i]^T$ is vector of the rotor shaft nodal points displacements. Substituting Eqs. (26) and (27) into identity (28) we get the disk matrices

$$\boldsymbol{M}_D = \begin{bmatrix} m & 0 & 0 & -ma \\ 0 & m & ma & 0 \\ 0 & ma & I + ma^2 & 0 \\ -ma & 0 & 0 & I + ma^2 \end{bmatrix} , \; \boldsymbol{G}_D = \begin{bmatrix} 0 & 0 & 0 & 0 \\ 0 & 0 & 0 & 0 \\ 0 & 0 & 0 & I_0 \\ 0 & 0 & -I_0 & 0 \end{bmatrix} , \tag{29}$$

$$\boldsymbol{B}_D = \mathrm{diag}[b_l, b_l, b_c, b_c] \,.$$

The mass, external damping and gyroscopic matrices of the rotor shaft with disks (turbine and compressor wheels, seal and trust rings) have structure

$$\boldsymbol{X}_R = \sum_e \boldsymbol{X}_e + \sum_D \boldsymbol{X}_D \,, \; \boldsymbol{X}_R = \boldsymbol{M}_R, \boldsymbol{B}_R^{(E)}, \boldsymbol{G}_R \,, \; \boldsymbol{X}_D = \boldsymbol{M}_D, \boldsymbol{B}_D, \boldsymbol{G}_D \,, \tag{30}$$

where the FE matrices (24) and the disk matrices (29) are localized on positions corresponding to coupling shaft nodal points displacements.

In order to reduce the bearing friction, the high-speed turbocharger is supported on the rotating floating ring bearings having the inner (I) and outer (O) oil films (Fig.3). We consider the rotor shaft rotation with constant angular velocity ω in the opposite direction around X axis. Using Lagrange's approach we derive the mass matrix of the rotating floating ring bearings. The kinetic energy of both

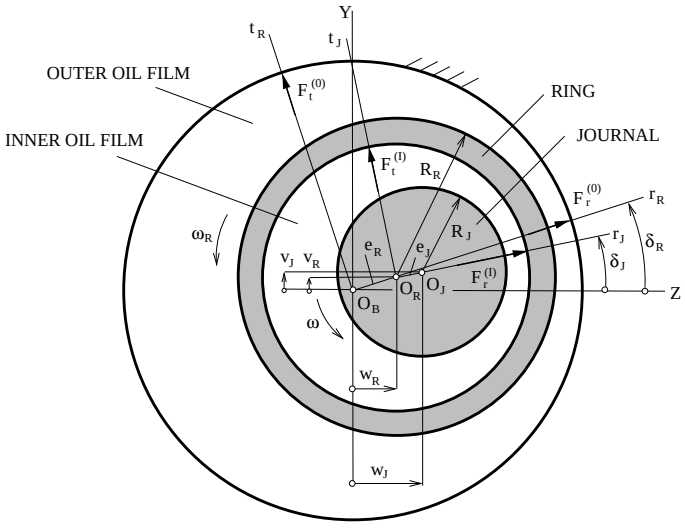

Fig. 3: Rotating floating ring bearing

rings, on condition lateral ring vibrations is

$$E_k^{(B)} = \frac{1}{2} m_a (\dot{v}_a^2 + \dot{w}_a^2) + \frac{1}{2} m_b (\dot{v}_b^2 + \dot{w}_b^2) \,, \tag{31}$$

where m_a, m_b are ring masses. The corresponding bearing mass matrix in the configuration space defined in (23) follows from identity

$$\frac{\partial E_k^{(B)}}{\partial \dot{\boldsymbol{q}}_B} = \boldsymbol{M}_B \dot{\boldsymbol{q}}_B \;\Rightarrow\; \boldsymbol{M}_B = \mathrm{diag}[m_a, m_a, m_b, m_b]\,. \tag{32}$$

The bearing forces $F_r^{(I)}$, $F_t^{(I)}$ and $F_r^{(O)}$, $F_t^{(O)}$ (see Fig.3) are based on the corresponding rotating coordinate system (Krämer (1993)) r_J, t_J and r_R, t_R of the journal (J) and ring(R). Therefore, the coordinate transformation from the rotating to inertial coordinate system Y, Z is necessary for the formulation of the motion equations

$$\begin{bmatrix} F_Y^{(I)} \\ F_Z^{(I)} \end{bmatrix} = \begin{bmatrix} \sin\delta_J & \cos\delta_J \\ \cos\delta_J & -\sin\delta_J \end{bmatrix} \begin{bmatrix} F_r^{(I)} \\ F_t^{(I)} \end{bmatrix}, \quad \begin{bmatrix} F_Y^{(O)} \\ F_Z^{(O)} \end{bmatrix} = \begin{bmatrix} \sin\delta_R & \cos\delta_R \\ \cos\delta_R & -\sin\delta_R \end{bmatrix} \begin{bmatrix} F_r^{(O)} \\ F_t^{(O)} \end{bmatrix}, \tag{33}$$

where δ_J, δ_R are angular positions of the journal and ring, respectively. Bearing force components in the rotating coordinates depend on the ε_J, $\dot{\varepsilon}_J$, $\dot{\delta}_J$, $\omega - \omega_R$ and ε_R, $\dot{\varepsilon}_R$, $\dot{\delta}_R$, ω_R nonlinearly (Krämer (1993), Shäfer (2012)), where ε_J, ε_R are the journal and ring relative eccentricities and ω, ω_R are the angular velocities of the rotor (journal) and bearing ring.

In case of linear rotordynamics the bearing forces $F_r^{(I)}$, $F_t^{(I)}$ and $F_r^{(O)}$, $F_t^{(O)}$ are linearized in the neighbourhood of the static equilibrium position. In case of the floating ring bearings the linearized forces are

$$\begin{bmatrix} F_Y^{(I)} \\ F_Z^{(I)} \end{bmatrix} = \begin{bmatrix} F_{0,Y}^{(I)} \\ F_{0,Z}^{(I)} \end{bmatrix} - \begin{bmatrix} k_{YY}(\omega) & k_{YZ}(\omega) \\ k_{ZY}(\omega) & k_{ZZ}(\omega) \end{bmatrix} \begin{bmatrix} \bar{v}_J - \bar{v}_R \\ \bar{w}_J - \bar{w}_R \end{bmatrix} - \begin{bmatrix} b_{YY}(\omega) & b_{YZ}(\omega) \\ b_{ZY}(\omega) & b_{ZZ}(\omega) \end{bmatrix} \begin{bmatrix} \dot{\bar{v}}_J - \dot{\bar{v}}_R \\ \dot{\bar{w}}_J - \dot{\bar{w}}_R \end{bmatrix}, \tag{34}$$

$$\begin{bmatrix} F_Y^{(O)} \\ F_Z^{(O)} \end{bmatrix} = \begin{bmatrix} F_{0,Y}^{(O)} \\ F_{0,Z}^{(O)} \end{bmatrix} - \begin{bmatrix} k_{YY}(\omega) & k_{YZ}(\omega) \\ k_{ZY}(\omega) & k_{ZZ}(\omega) \end{bmatrix} \begin{bmatrix} \bar{v}_R \\ \bar{w}_R \end{bmatrix} - \begin{bmatrix} b_{YY}(\omega) & b_{YZ}(\omega) \\ b_{ZY}(\omega) & b_{ZZ}(\omega) \end{bmatrix} \begin{bmatrix} \dot{\bar{v}}_R \\ \dot{\bar{w}}_R \end{bmatrix}, \tag{35}$$

where $\bar{v}_J$, $\bar{w}_J$ and $\bar{v}_R$, $\bar{w}_R$ are displacements of the journal and ring centres from the static equilibrium position resulted from static load of the journals and bearing rings.

The bearing oil stiffness and damping coefficients in Eqs. (34) and (35) can be in the first approximation expressed depending on relative journal speed with respect to bearing ring $\omega - \omega_R$ and on bearing ring speed ω_R. So-called the ring speed ratio $RSR = \frac{\omega_R}{\omega}$ at the steady state condition depends on dynamic viscosity of the inner and outer oil-films, geometrical parameters of the bearing ring and inner and outer radial bearing clearance (Shäfer (2012)). As a result of specific ring speed ratio in steady state conditions (constant ω) the stiffness and damping matrices of the inner and outer oil-films in Eqs. (34) and (35) depend on ω. We describe them as $\boldsymbol{K}_x^{(I)}(\omega)$, $\boldsymbol{B}_x^{(I)}(\omega)$ for inner oil-film and $\boldsymbol{K}_x^{(O)}(\omega)$, $\boldsymbol{B}_x^{(O)}(\omega)$ for outer oil-film of the left ($x = a$) and right ($x = b$) bearings. The changes of the bearing forces relating to small displacements and velocities of the rotor from static equilibrium positions, expressed by the second and the third components in Eqs. (34) and (35), in the global coordinate system defined in (22) can be expressed in the matrix form

$$\Delta \boldsymbol{f}_B = \begin{bmatrix} \vdots \\ -\Delta F_{Y,a}^{(I)} \\ -\Delta F_{Z,a}^{(I)} \\ \vdots \\ -\Delta F_{Y,b}^{(I)} \\ -\Delta F_{Z,b}^{(I)} \\ \vdots \\ - - - \\ \Delta F_{Y,a}^{(I)} - \Delta F_{Y,a}^{(O)} \\ \Delta F_{Z,a}^{(I)} - \Delta F_{Z,a}^{(O)} \\ \Delta F_{Y,b}^{(I)} - \Delta F_{Y,b}^{(O)} \\ \Delta F_{Z,b}^{(I)} - \Delta F_{Z,b}^{(O)} \end{bmatrix} = -\boldsymbol{K}_B(\omega) \begin{bmatrix} \bar{\boldsymbol{q}}_R \\ \bar{\boldsymbol{q}}_B \end{bmatrix} - \boldsymbol{B}_B(\omega) \begin{bmatrix} \dot{\bar{\boldsymbol{q}}}_R \\ \dot{\bar{\boldsymbol{q}}}_B \end{bmatrix}, \tag{36}$$

where $\bar{\boldsymbol{q}}_R$, $\bar{\boldsymbol{q}}_B$ are vectors of rotor shaft and bearing rings displacements from the static equilibrium position. According to (34) and (35) the stiffness and damping matrices of the two separated oil-films of both bearings are localized in global matrices according to vectors $\bar{\boldsymbol{q}}_{J_x} = [\bar{v}_{J_x}, \bar{w}_{J_x}]^T$, $\bar{\boldsymbol{q}}_{R_x} = [\bar{v}_{R_x}, \bar{w}_{R_x}]^T$, $x = a, b$ as follows

$$\boldsymbol{K}_B(\omega) = \begin{bmatrix} \boldsymbol{K}_a^{(I)} & & -\boldsymbol{K}_a^{(I)} & \\ & \boldsymbol{K}_b^{(I)} & & -\boldsymbol{K}_b^{(I)} \\ -\boldsymbol{K}_a^{(I)} & & \boldsymbol{K}_a^{(I)} + \boldsymbol{K}_a^{(O)} & \\ & -\boldsymbol{K}_b^{(I)} & & \boldsymbol{K}_b^{(I)} + \boldsymbol{K}_b^{(O)} \end{bmatrix} \begin{matrix} \}\bar{\boldsymbol{q}}_{J_a} \\ \}\bar{\boldsymbol{q}}_{J_b} \\ \}\bar{\boldsymbol{q}}_{R_a} \\ \}\bar{\boldsymbol{q}}_{R_b} \end{matrix} ; \; \boldsymbol{B}_B(\omega) \sim \boldsymbol{K}_B(\omega) . \quad (37)$$

The linearized motion equations of the turbochargers (Fig.1), according to (30), (32) and (36) can be written as

$$\begin{bmatrix} \boldsymbol{M}_R & \boldsymbol{0} \\ \boldsymbol{0} & \boldsymbol{M}_B \end{bmatrix} \begin{bmatrix} \ddot{\bar{\boldsymbol{q}}}_R \\ \ddot{\bar{\boldsymbol{q}}}_B \end{bmatrix} + \left(\begin{bmatrix} \boldsymbol{B}_R^{(E)} + \boldsymbol{B}_R^{(I)} - \omega \boldsymbol{G}_R & \boldsymbol{0} \\ \boldsymbol{0} & \boldsymbol{0} \end{bmatrix} + \boldsymbol{B}_B(\omega) \right) \begin{bmatrix} \dot{\bar{\boldsymbol{q}}}_R \\ \dot{\bar{\boldsymbol{q}}}_B \end{bmatrix} +$$

$$+ \left(\begin{bmatrix} \boldsymbol{K}_R - \omega \boldsymbol{C}_R & \boldsymbol{0} \\ \boldsymbol{0} & \boldsymbol{0} \end{bmatrix} + \boldsymbol{K}_B(\omega) \right) \begin{bmatrix} \bar{\boldsymbol{q}}_R \\ \bar{\boldsymbol{q}}_B \end{bmatrix} = \begin{bmatrix} \boldsymbol{f}_R(t) \\ \boldsymbol{0} \end{bmatrix} , \quad (38)$$

where $\boldsymbol{f}_R(t)$ is vector of the unbalance of disks (turbine and compressor wheels).

4. Application

The homogenous motion equations (38) (for $\boldsymbol{f}_R(t) = \boldsymbol{0}$) was applied on eigenvalues calculation of the small automotive turbocharger with rotor mass 0.1[kg]. The rotor discretized into 13 nodes (Fig.1) is supported on two short cylindrical floating ring bearings. The eigenvalues λ_ν are found by solving the eigenvalue problem

$$(\boldsymbol{A} - \lambda \boldsymbol{E})\boldsymbol{u} = \boldsymbol{0} \quad (39)$$

in state space $\boldsymbol{u} = [\dot{\bar{\boldsymbol{q}}}, \bar{\boldsymbol{q}}]^T$, where non-symmetric system matrix is

$$\boldsymbol{A} = \begin{bmatrix} -\boldsymbol{M}^{-1}\boldsymbol{B}(\omega) & -\boldsymbol{M}^{-1}\boldsymbol{K}(\omega) \\ \boldsymbol{E} & \boldsymbol{0} \end{bmatrix} \quad (40)$$

and $\boldsymbol{M}$, $\boldsymbol{B}(\omega)$, $\boldsymbol{K}(\omega)$ are global matrices of order $n = 56$ in the motion equations (38). The bearing stiffness and damping coefficients were calculated by means of bearing dimensionless stiffness κ_{ij} and damping β_{ij} coefficients (Krämer (1993), Shäfer (2012)) using the Reynolds lubrication equation for radial cylindrical short bearings with the non-cavitating oil-films. The bearing forces were linearized by using the Taylor's series at the journal and bearing rings static equilibrium positions. The bearing inner and outer oil-film coefficients of both bearings in equations (34) and (35) were calculated for the static load at equilibrium, constant rotor speed ω and ring speed ratio for the concrete oil and geometrical bearing parameters. The dynamic oil viscosities of the lubricating inner and outer oil-films versus temperature were calculated using the Cameron and Vogel equation (Shäfer (2012)).

The linearized mathematical model of the rotor has besides complex conjugate pairs of eigenvalues also even number of real values representing nonoscillatory overdamping modes. The real part of two low-frequency eigenvalues is positive however their imaginary parts are much smaller than the rotor speed. The Campbell diagram displayed at Fig.4 expresses the dependence of the eigenfrequencies (imaginary parts of the complex eigenvalues) of the turbocharger on rotor speed $n = \frac{30\omega}{\pi}$ [rpm]. The critical speeds n_k [rpm], where the eigenfrequencies cuts the synchronous excitation line, can be calculated as roots of the nonlinear equation

$$n = \frac{30}{\pi} \mathrm{Im}\{\lambda_\nu(n)\} . \quad (41)$$

The calculated critical speeds in the investigated rotor speed range $n \in \langle 24000, 240000 \rangle$ [rpm] are given in Table 1. The rotor unbalance, caused by the static unbalance of the turbine and compressor wheels with different angular phase α_C between unbalanced turbine and compressor wheel vectors, can

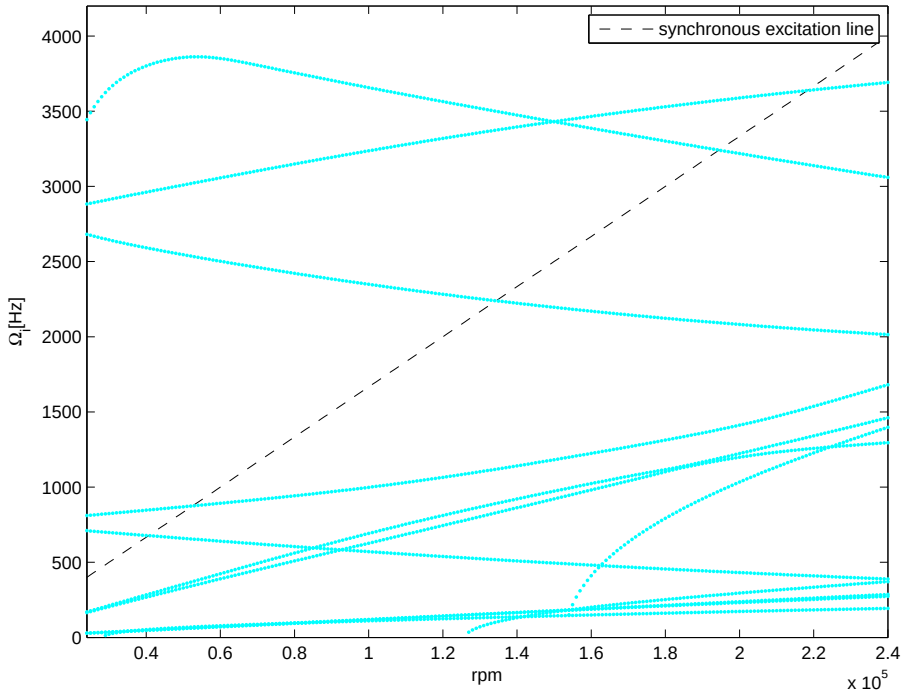

Fig. 4: Campbell diagram of the turbocharger

Tab. 1: Critical speed of the rotor (B=backward, F=forward) without and with strengthening of the shaft in area of the compressor wheel

Critical speeds					
order	without strengthening		with strengthening		
	f[Hz]	n[rpm]	f[Hz]	n[rpm]	
1	677.38	40643	712.94	42776	B
2	875.20	52512	889.71	53377	F
3	2239.38	134363	2483.76	149026	B
4	3241.25	194475	4865.54	291932	B
5	3637.61	218257	5436.85	326211	F

be expressed in equations (38) by the complex form

$$\tilde{\boldsymbol{f}}_R(t) = \tilde{\boldsymbol{f}}_R \mathrm{e}^{\mathrm{i}\omega t}\,;\;\; \tilde{\boldsymbol{f}}_R = \omega^2 \begin{bmatrix} m_T e_T \\ \mathrm{i} m_T e_T \\ \mathrm{i} m_T e_T a \\ -m_T e_T a \\ \vdots \\ m_C e_C \mathrm{e}^{\mathrm{i}\alpha_C} \\ \mathrm{i} m_c e_C \mathrm{e}^{\mathrm{i}\alpha_C} \\ \vdots \end{bmatrix} \begin{matrix} \ldots 1 \\ \ldots 2 \\ \ldots 3 \\ \ldots 4 \\ \\ \ldots 33 \\ \ldots 34 \\ \end{matrix} \;\; ; \;\; \mathrm{i} = \sqrt{-1}\,, \tag{42}$$

where $m_T e_T$, $m_C e_C$ [kgm] are corresponding unbalances. According to (38) the vector of complex amplitudes of the rotor steady state displacements $\tilde{\boldsymbol{q}} = [\tilde{\boldsymbol{q}}_R, \tilde{\boldsymbol{q}}_B]$ from static equilibrium position is

$$\tilde{\boldsymbol{q}} = [-\boldsymbol{M}\omega^2 + \mathrm{i}\omega \boldsymbol{B}(\omega) + \boldsymbol{K}(\omega)]^{-1} \begin{bmatrix} \tilde{\boldsymbol{f}}_R \\ \boldsymbol{0} \end{bmatrix}. \tag{43}$$

The turbine and compressor wheel amplitudes of lateral displacements versus rotor speed caused by the permissible residual unbalance according to standard DIN-ISO 1940 (Shäfer (2012)) $m_T e_T$ =0.1 [gmm], $m_c e_C$=0.05 [gmm] are displayed in Fig.5 and Fig.6. The unbalance generates resonances at neighbourhood of critical speeds.

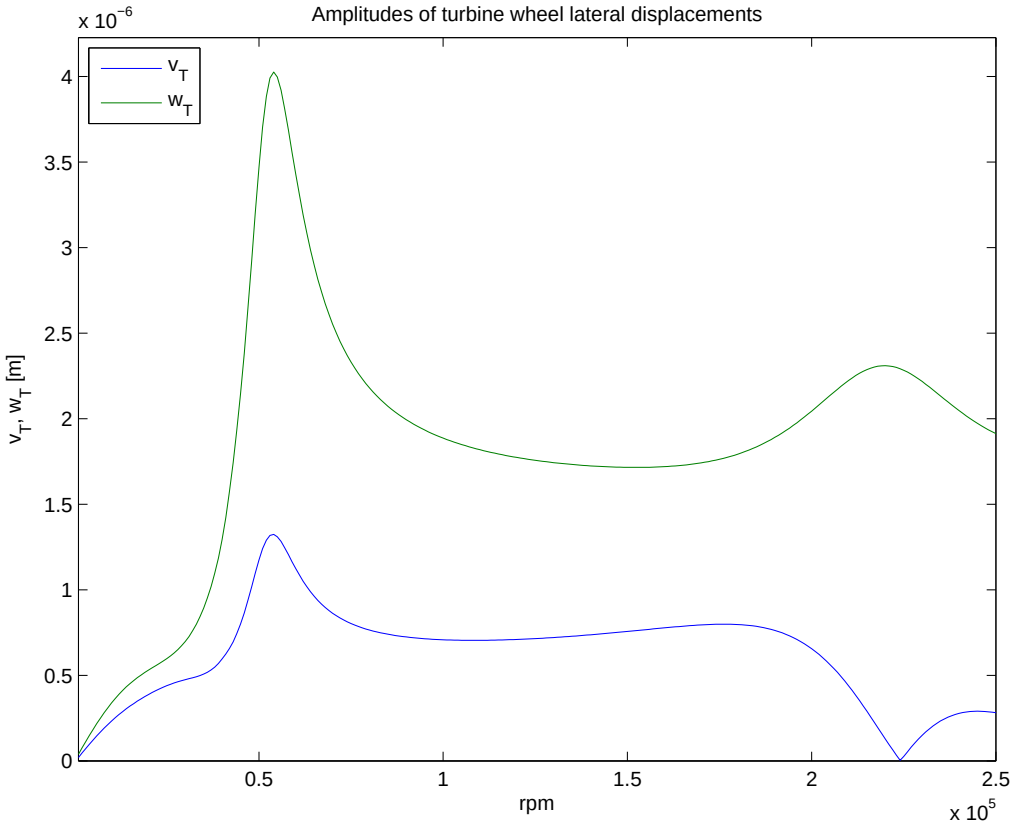

Fig. 5: Amplitudes of turbine wheel centre lateral displacements for balancing quality grade G40 of the DIN-ISO 1940 and $\alpha_C = 0$

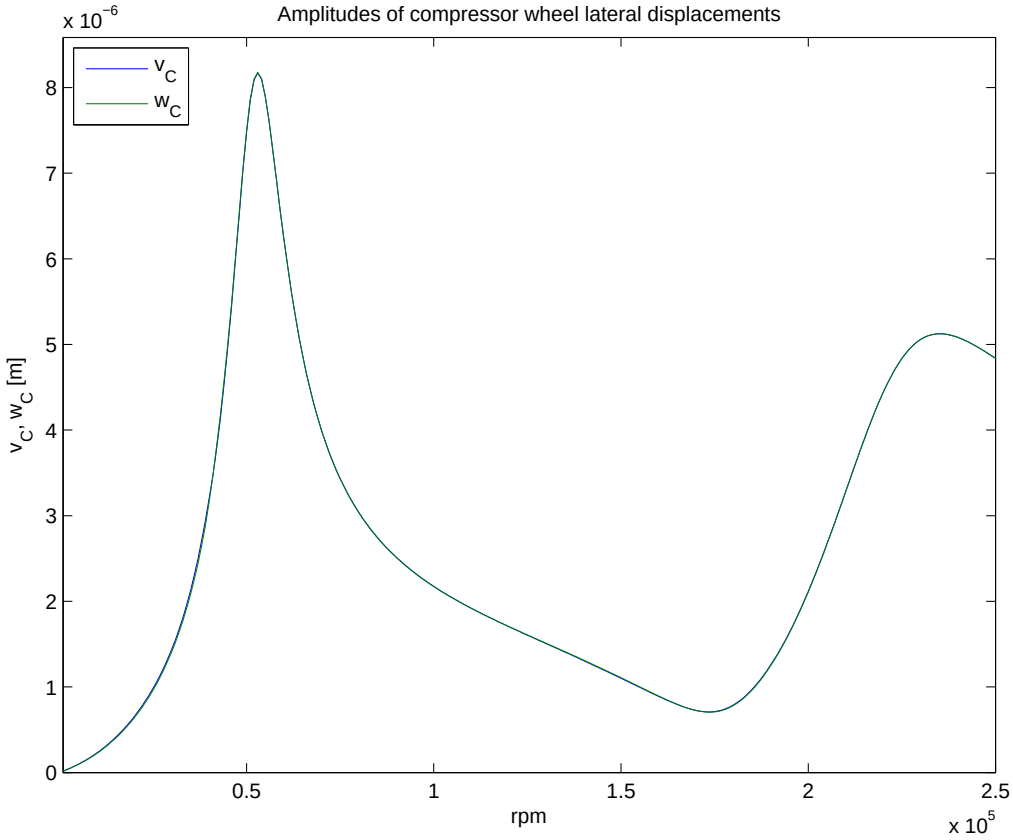

Fig. 6: Amplitudes of compressor wheel centre lateral displacements for balancing quality grade G40 of the DIN-ISO 1940 and $\alpha_C = 0$

5. Conclusion

The described method was applied to investigate the complex eigenvalues, stability, unbalance response and critical speeds of the well-balanced concrete turbocharger rotor supported on two floating ring bearings. The computer program in MATLAB code makes it possible to analyse an influence of design and operation parameters of the turbochargers on these phenomenons. The adjusted nonlinear mathematical model including nonlinear characteristics of the bearing forces will be used for vibration analysis at the large journals and floating bearing rings deflections.

Acknowledgement

This work was supported by the European Regional Development Fund (ERDF), project "NTIS", European Centre of Excellence, CZ.1.05/1.1.00/02.0090.

References

Byrtus, M., Hajžman, M. & Zeman, V. (2010) *Dynamika rotujících soustav.* Monograph. UWB, Pilsen.

Gash, R., Pfützner, H. (1975) *Rotordynamik.* Springer, Berlin.

Genta, G. (2005) *Dynamics of Rotating Systems.* Springer, Heidelberg.

Krämer, E. (1993) *Dynamics of Rotors and Foundations.* Springer, Berlin.

Muszińska, A. (2005) *Rotordynamics.* CRC Press Taylor & Francis, Boca Raton.

Shäfer, H. N. (2012) *Rotordynamics of Automotive Turbochargers.* Springer, Heidelberg.

Šimek, J. (2013), Some interesting features of turbocharger rotor dynamics. In: *Proc. of Colloquium Dynamic of Machines 2013* (Pešek ed). Praque, pp. 111-116.

Yamamoto, T., Ishida, Y. (2001) *Linear and Nonlinear Rotordynamics.* John Wiley & Sons, New York.

Zeman, V., Rendlová, Z. (2011) Stability analysis of the rotor vibration with external and internal damping. *Modelling and Optimization of Physical systems*, 10, Gliwice, pp. 89-96.